The internal ballistics analysis of underwater solid motor with protective nozzle caps

Nguyen Truong Thanh[1*], Nguyen Van Hung[2], Vu Cao Ky[2]

[1]Institute of Missile, Academy of Military Science and Technology, 17 Hoang Sam, Nghia Do, Hanoi, Vietnam;
[2]Le Quy Don University, 236 Hoang Quoc Viet, Nghia Do, Hanoi, Vietnam.
[*]Corresponding author: thanhvtv2010@gmail.com
Received 29 Nov. 2025; Revised 26 Jan. 2026; Accepted 10 Apr. 2026; Published 25 Apr. 2026.
DOI: https://doi.org/10.54939/1859-1043.j.mst.110.2026.169-176

ABSTRACT

This paper investigates the performance of a solid motor (SM) operating in underwater environments, specifically accounting for the influence of the protective nozzle closure cap assembly. A mathematical model for the internal ballistics is established, incorporating the critical phase of the seal-breaking process. During this stage, the partial combustion of the propellant increases the combustion chamber pressure, leading to the failure of the pressure seal. Concurrently, a portion of the combustion gas flows into the cavity formed between the closure cap and the nozzle, resulting in a pressure buildup within this region. Once the pressure in the low-pressure cavity reaches a threshold sufficient to shear the retaining bolts, the closure cap is jettisoned. Following the ejection of the cap, the combustion gases are discharged through the nozzle into the surrounding medium, transitioning the SM into its conventional operating mode. The findings of this study provide a theoretical foundation for the calculation, design, and structural fabrication of a solid motor intended for underwater applications.

Keywords: Solid motor; High-pressure chamber; Low -pressure chamber; Underwater solid motor; Internal ballistics.

1. INTRODUCTION

Solid motors have attracted sustained research interest owing to their structural simplicity, high reliability, and favorable thrust-to-weight ratio. Studies [1, 2] established fundamental methodologies for gas dynamics analysis, stagnation parameter evaluation, and thrust prediction in SMs. Subsequent work [3] developed internal ballistics models incorporating combustion heat release and thermal losses through motor walls, leading to optimized nozzle and motor structural designs. Design-oriented investigations for various missile applications were reported in [8–10], with particular emphasis on loading coefficients and structural optimization. In addition, inverse internal ballistics problems aimed at identifying propellant grain parameters were addressed in [4].

Beyond conventional operating conditions, several studies have examined SM performance in specialized environments. The influence of water depth on thrust characteristics was investigated in [5]. Moreover, H. T. Dung [6] analyzed the effects of chamber parameters on SM performance by accounting for multiphase flow phenomena, specifically the presence of solid particles in aluminum-powdered propellants, and demonstrated a noticeable reduction in thrust due to the solid phase.

When operating in underwater environments, SMs are subjected to ambient conditions that differ fundamentally from those encountered in the atmosphere. To ensure safe operation and prevent water ingress, such motors are commonly equipped with a sealed nozzle protective cap assembly. This configuration alters the boundary conditions at the nozzle exit, thereby modifying the internal pressure evolution and exhaust flow characteristics during the launch process. Consequently, a rigorous investigation of the internal ballistics of SMs during the underwater launch process, with explicit consideration of the protective nozzle closure cap, is required. The present study aims to address this issue and to provide a scientific basis for the theoretical analysis and engineering design of solid motors intended for underwater applications.

2. INTERNAL BALLISTICS MODELING AND GOVERNING EQUATIONS

2.1. Modeling of physical processes in motor operation

Processes occurring during solid fuel engine operation in a water environment are modeled as shown in figure 1. This model includes the engine combustion chamber 1 (high-pressure chamber) and the intermediate chamber 4, formed by the nozzle's bottom and a sealing cap (low-pressure chamber).

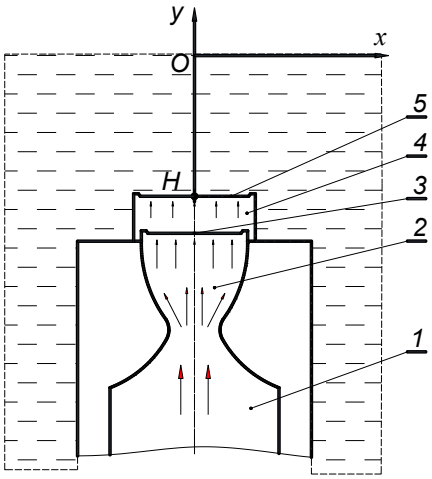

Figure 1. *Schematic of a solid motor with a nozzle closure cap assembly*
1. Combustion chamber; 2. Nozzle; 3. Nozzle closure cap;
4. Intermediate chamber; 5. Sealing cap.

The operating process of the solid motor can be divided into three distinct phases. Phase I corresponds to the period during which the sealing cap (5) remains confined within the motor and has not yet been ejected into the surrounding environment. Phase II begins immediately after the sealing cap (5) is released into the ambient medium. Phase III, referred to as the free exhaust phase, starts when propellant combustion is completed and continues until the chamber pressure equilibrates with the ambient pressure.

2.2. Fundamental assumptions

- To simplify the mathematical model, the following assumptions are adopted:

- The propellant burns completely and follows a geometric burning law, and the burning rate obeys the exponential Saint Robert's law.

- The adiabatic exponent (γ) and the gas constant (R) are assumed to remain constant throughout the entire process.

- The ignition transient phase is neglected.

- The after-effect (tail-off) phase of the combustion gases is neglected.

- Frictional forces between the sealing cap and the housing walls are neglected.

- The launching process is conducted under standard ambient and environmental conditions.

2.3. Internal ballistics formulation

The internal ballistics of the solid motor operating in an underwater environment are formulated by dividing the operating process into three distinct stages: Phase I: Sealing cap ejection phase; Phase II: Normal underwater motor operation; Phase III: Free gas discharge phase.

2.3.1. Phase I: Sealing cap ejection phase

The governing equations describing the motor operation during the sealing cap ejection phase are established [2, 3, 7] as follows.

$$\begin{cases} 1.\dfrac{d\psi}{dt}=\dfrac{S\cdot u\cdot \rho_T}{\omega};\quad 2.\dfrac{d\chi_n}{dt}=\dfrac{a\cdot b}{\left(1+b\cdot\psi\right)^2}.\dfrac{d\psi}{dt};\qquad 3.\dfrac{dm_{b1}}{dt}=\dot{m}_{tp}-\dot{m}_{td12};\\ 4.\dfrac{dp_{b1}}{dt}=\dfrac{R}{w_1}.\left(T_{b1}.\chi_n.\dfrac{dm_{b1}}{dt}+m_{b1}.\chi_n.\dfrac{dT_{b1}}{dt}+m_{b1}.T_{b1}.\dfrac{d\chi_n}{dt}-\dfrac{m_{b1}\cdot\chi_n\cdot T_{b1}}{w_1}.S.u\right);\\ 5.\dfrac{dT_{b1}}{dt}=\dfrac{T_1}{m_{b1}}.\dot{m}_{tp}-\dfrac{k\cdot T_{b1}\cdot\dot{m}_{td12}}{m_{b1}}-\dfrac{dm_{b1}}{dt}.\dfrac{T_{b1}}{m_{b1}};\quad 6.\dfrac{dm_{b2}}{dt}=\dot{m}_{td12}-\dot{m}_{td23};\\ 7.\dfrac{dp_{b2}}{dt}=\dfrac{R}{w_2}.\left(T_{b2}.\chi_n.\dfrac{dm_{b2}}{dt}+m_{b2}.\chi_n.\dfrac{dT_{b2}}{dt}+m_{b2}.T_{b2}.\dfrac{d\chi_n}{dt}-\dfrac{m_{b2}.\chi_n.T_{b2}}{w_2}.S_d.v_d\right);\\ 8.\dfrac{dT_{b2}}{dt}=\dfrac{k\cdot T_{b1}}{m_{b2}}.\dot{m}_{td12}-\dfrac{k\cdot T_{b2}}{m_{b2}}.\dot{m}_{td23}-\dfrac{dm_{b2}}{dt}.\dfrac{T_{b2}}{m_{b2}}-\dfrac{\phi_m\cdot\left(k-1\right)\cdot m_d\cdot v_d}{R\cdot m_{b2}}.\dfrac{dv_d}{dt};\\ 9.dw_2=S_d\cdot dl_d;\qquad 10.\dfrac{dv_d}{dt}=\dfrac{S_d\cdot p_{b2}}{\phi_m\cdot m_d};\quad 11.\dfrac{dl_d}{dt}=v_d; \end{cases} \tag{1}$$

Where: ω: is the initial mass of the propellant (*kg*); *u*: is the burning rate of the propellant (*m/s*); ρ_T : is the density of the propellant *(kg/m*^{3}); *S(e)*: is the burning surface area of the propellant at the considered time (*m*^{2}); *a* and *b* are the geometric shape factors of the propellant; $\dot{m}_{b1}$: The rate of change of gas mass remaining in the high-pressure chamber; $\dot{m}_{tp}$: The gas mass flow rate generated by the propellant combustion in the high-pressure chamber; w_1 denotes the gas volume in the high-pressure chamber; T_1: enotes the constant-pressure combustion temperature of the combustion gases; w_2: denotes the volume of the combustion gases in the intermediate chamber (*m*^{3}); $m_{b2:}$ denotes the mass of the combustion gases in the intermediate chamber (*kg*); χ_n : denotes the heat loss in the intermediate chamber; v_d: denotes the translational velocity of the water-sealing cap; $S_{d:}$ denotes the internal effective area of the water-sealing cap; dw_2 : denotes the incremental increase in the volume of the intermediate chamber over a time interval *dt*; $l_{d:}$ denotes the displacement of the water-sealing cap; m_d: denotes the mass of the water-sealing cap (*kg*); ϕ_m : denotes the mass augmentation coefficient of the sealing cap; $\dot{m}_{td12}$: The gas mass flow rate discharged through the nozzle into the intermediate chamber;

- If the pressure differential satisfies the condition $1\le\dfrac{p_{b1}}{p_{b2}}<\left(\dfrac{k+1}{2}\right)^{\frac{k}{k-1}}$ the gas flow from the high-pressure chamber to the intermediate chamber is subsonic (less than the local speed of sound). In this case, the mass flow rate is determined by the following equation:

$$\dot{m}_{td12}=\frac{\phi_2.F_{12}.p_{b1}}{\sqrt{\chi_n.R.T_{b1}}}\cdot\sqrt{\frac{2k}{k-1}\cdot\left(\left(\frac{p_{b2}}{p_{b1}}\right)^{\frac{2}{k}}-\left(\frac{p_{b2}}{p_{b1}}\right)^{\frac{k+1}{k}}\right)} \tag{2}$$

- If the pressure ratio is $\dfrac{p_{b1}}{p_{b2}}\ge\left(\dfrac{k+1}{2}\right)^{\frac{k}{k-1}}$ the gas flow from the high-pressure chamber to the intermediate chamber reaches sonic velocity. At this condition, the mass flow rate is maximized (choked flow) and is calculated by the following formula:

$$\dot{m}_{td12} = \frac{\phi_2 . K_0(K) . F_{12} . p_{b1}}{\sqrt{\chi_n . R . T_{b1}}} \tag{3}$$

with: p_{b1}: combustion gas pressure in the high-pressure chamber (Pa); p_{b2}: combustion gas pressure in the intermediate chamber (Pa); ϕ_2: energy loss coefficient; χ_n: eat loss in the high-pressure chamber; $K_0(K)$: adiabatic exponent function: $K_0(K) = \left(\frac{2}{k+1}\right)^{\frac{1}{k-1}} \cdot \sqrt{\frac{2 \cdot k}{k+1}}$, adiabatic index k of the combustion gas; T_{b1}: combustion gas temperature in the high-pressure chamber (K); R: gas constant of the combustion products; F_{12}: throat area (or critical cross-sectional area) of the high-pressure chamber nozzle.

$\dot{m}_{b2}$: denotes the rate of change of the gas mass stored in the intermediate chamber; $\dot{m}_{td23}$: denotes the gas mass flow rate discharged from the intermediate chamber into the ambient environment.

- If the pressure difference satisfie $1 \le \frac{p_{b2}}{p_{mt}} < \left(\frac{k+1}{2}\right)^{\frac{k}{k-1}}$ tthe gas discharged from the intermediate chamber into the ambient environment occurs at a **subsonic velocity** (i.e., lower than the local speed of sound). In this case, the gas mass flow rate can be expressed as:

$$\dot{m}_{td23} = \frac{\phi_2 . F_{23} . p_{b2}}{\sqrt{\chi_n . R . T_{b2}}} \cdot \sqrt{\frac{2k}{k-1} \cdot \left(\left(\frac{p_{mt}}{p_{b2}}\right)^{\frac{2}{k}} - \left(\frac{p_{mt}}{p_{b2}}\right)^{\frac{k+1}{k}} \right)} \tag{4}$$

- If the pressure difference satisfies $\frac{p_{b2}}{p_{mt}} \ge \left(\frac{k+1}{2}\right)^{\frac{k}{k-1}}$ the gas discharged from the intermediate chamber into the ambient environment reaches sonic conditions (choked flow). In this case, the gas mass flow rate attains its maximum value and is given by:

$$\dot{m}_{td23} = \frac{\phi_2 . K_0(K) . F_{23} . p_{b2}}{\sqrt{\chi_n . R . T_{b2}}} \tag{5}$$

with: p_{mt}: denotes the ambient pressure; F_{23}: denotes the effective area of the sealing cap; T_{b2}: denotes the combustion gas temperature in the intermediate chamber.

2.3.2. Phase II: Motor operation in an underwater environmen

During this stage, the water-sealing cap has been completely expelled into the surrounding environment. Combustion products generated in the combustion chamber are discharged through the nozzle into the ambient water. Under these conditions, the state equations of the high-pressure chamber can be written as:

$$\begin{gathered}
1.\frac{d\psi}{dt} = \frac{S \cdot u \cdot \rho_T}{\omega}; \qquad 2.\frac{d\chi_n}{dt} = \frac{a \cdot b}{\left(1 + b \cdot \psi\right)^2} . \frac{d\psi}{dt}; \qquad 3.\frac{dm_{b1}}{dt} = \dot{m}_{tp} - \dot{m}_{td12}; \\
4.\frac{dp_{b1}}{dt} = \frac{R}{w_1} . \left(T_{b1} . \chi_n . \frac{dm_{b1}}{dt} + m_{b1} . \chi_n . \frac{dT_{b1}}{dt} + m_{b1} . T_{b1} . \frac{d\chi_n}{dt} - \frac{m_{b1} \cdot \chi_1 \cdot T_{b1}}{w_1} . S . u \right); \\
5.\frac{dT_{b1}}{dt} = \frac{T_1}{m_{b1}} . \dot{m}_{tp} - \frac{k \cdot T_{b1} \cdot \dot{m}_{td12}}{m_{b1}} - \frac{dm_{b1}}{dt} \cdot \frac{T_{b1}}{m_{b1}}
\end{gathered} \tag{6}$$

2.3.3. Phase III (free gas discharge phase)

After the propellant is fully consumed, the governing system of equations reduces to:

$$\begin{cases} 1.\dfrac{d\psi}{dt}=0; \quad 2.\dfrac{d\chi_n}{dt}=0; \quad 3.\dfrac{dm_{b1}}{dt}=\dfrac{\phi_2.K_0(k).F_{12}.p_{b1}}{\sqrt{R.T_{b1}}}; \\ 4.\dfrac{dp_{b1}}{dt}=\dfrac{k.\dot{m}_{b1}R.T_{b1}}{w_1}; \quad 5.\dfrac{dT_{b1}}{dt}=-(k-1)\phi_2.K_0(k).F_{12}.\sqrt{R.T_{b1}}\dfrac{T_{b1}}{w_1}. \end{cases} \tag{7}$$

The coupled systems of differential equations, Equations (1), (6), and (7), are solved using the Runge–Kutta method, subject to the corresponding initial conditions.

3. NUMERICAL RESULTS AND DISCUSSION

3.1. Comparison between computational and experimental results

Underwater launch characteristics of a solid-fuel engine were calculated at a 10-m immersion depth. Utilizing the parameters defined in Table 1, the computational results are presented in Table 2 and illustrated in Figures 2 and 3.

Table 1. *Launch parameters of the solid motor.*

TT	Parameters	Symbol	Value	Unit
1	Outer diameter of the propellant grain	D	104,5	mm
2	Inner diameter of the propellant grain	d	18,0	mm
3	Length of the propellant grain	L	950	mm
4	Propellant density	ρ_T	1580	kg/m^3
5	Burning-rate coefficient	u_1	40,8.10^{-6}	m/s
6	Adiabatic exponent	k	1,25	
7	Burning-rate exponent	ν	0,3435	
8	Ambient temperature correction coefficient	K_T	0,0034	
9	Erosive burning coefficient	K_w	10^{-6}	
10	Inner diameter of the combustion chamber	D_k	114	mm
11	Length of the combustion chamber	L_k	1020	mm
12	Throat diameter of the nozzle	d_{th}	34; 35	mm
13	Exit diameter of the nozzle	d_a	72	mm

By solving the systems of differential Equations (1), (6), and (7) numerically, the principal operating parameters of the launch motor are obtained and summarized in Table 2, with corresponding trends illustrated in Figures 2 and 3.

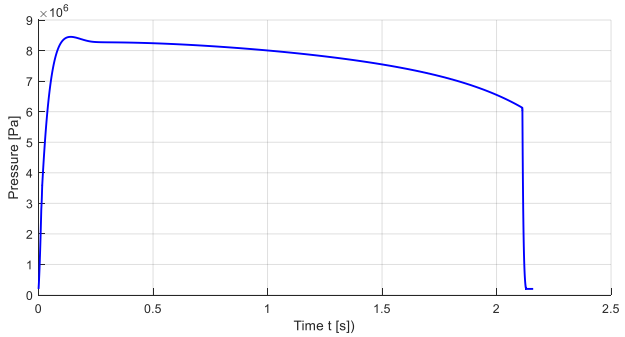

Figure 2. *Pressure graph vs. throat diameter d_{th} = 34 mm.*

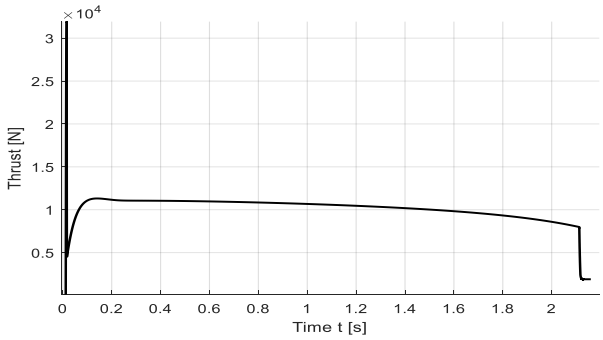

Figure 3. *Thrust graph vs. throat diameter d_{th} = 34mm.*

Table 2. *Calculated internal ballistic parameters for various throat diameters at an underwater depth of 10 m.*

Nozzle throat diameter (mm)	Maximum pressure (Mpa)	Average pressure (MPa)	Maximum thrust (N)	Average thrust (N)	Burning duration (s)	Total impulse (N.s)
33	9,34	7,75	32259	10234	2,062	21984,8
34	8,65	7,54	32566	10229	2,085	21781,4
34,5	8,32	7,32	32183	10120	2,091	21697,1
35	8,64	7,12	32645	10050	2,117	21575,5
36	7,48	6,63	32294	9795	2,171	21436,6

The experimental results for the solid-fuel motor at immersion depths below 10m are presented in Table 3 and illustrated in Figure 4.

Table 3. *Comparison between numerical simulation and experimental results for motor parameters.*

Number	Nozzle throat diameter d_{th} (mm)	Maximum thrust (N)	Average thrust (N)	Total impulse (N.s)	Burning duration (s)
No. 1	35	30032,1	10513,0	22318,1	2,15
No. 2	34	30088,7	10622,8	22653,3	2,12

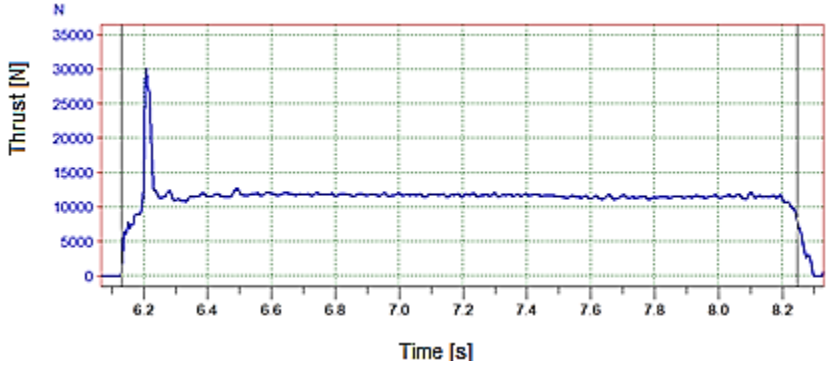

Figure 4. *Thrust graph vs. throat diameter d_{th} = 34mm.*

*Remarks:

+ During the sealing cap opening phase, the thrust of the motor increases rapidly and reaches

its maximum value. This peak thrust exceeds the average thrust by more than 300%. In this phase, the motor operates in a manner analogous to a coupled high-pressure chamber (combustion chamber) and low-pressure chamber (intermediate cavity), resulting in a pronounced transient thrust enhancement.

+ After the sealing cap has been completely ejected, the solid motor operates under normal conditions. The combustion products are discharged into the surrounding water through the nozzle in a manner similar to operation in an atmospheric environment.

3.2. Discussion of numerical results and experimental validation

Experimental measurements of the thrust–time history of the solid motor operating at a water depth of 10 m were obtained in a test tank. These results constitute an important and reliable scientific basis for comparison with the numerical predictions derived from the theoretical model based on the actual motor configuration.The numerical results show good agreement with the experimental data. This agreement demonstrates the validity of the proposed model from both qualitative and quantitative perspectives:

+ Qualitatively, the description of the motor operating principle before and after the separation of the sealing cap, represented as a sequence of distinct physical processes, is consistent with the observed experimental behavior.

+ Quantitatively, the theoretical model predicts the key internal launch parameters with high accuracy, including thrust level, motor operating time, and total impulse. The discrepancy between numerical and experimental results remains below 5%.

4. CONCLUSIONS

This study proposes a staged modeling framework to investigate the underwater launch dynamics of a solid-fuel motor. By integrating fundamental physical laws with the specific mechanical processes of the sealing cap deployment, a comprehensive internal ballistic model was formulated. The principal contributions of this research are as follows:

Mathematical Modeling: A robust mathematical model and its corresponding numerical solution procedure were established, specifically incorporating the structural configuration and opening mechanism of the water-sealing protective cap.

Model Validation: A comparative analysis between numerical simulations and experimental data was performed. The high degree of correlation between the predicted and measured performance parameters validates the accuracy and reliability of the proposed theoretical framework.

The findings of this study establish a rigorous scientific basis for the computational analysis, design optimization, and manufacturing of solid-fuel motors for underwater applications.

REFERENCES

[1]. Tran D. Dien, *"Internal Ballistics of Special Weapons"*, vols. 1–2, Military Technical University, Hanoi, Vietnam, (1975).

[2]. Pham T. Phiet, *"Theory of Rocket Engines"*, Military Technical Academy, Hanoi, Vietnam, (2006).

[3]. Dang H. Trien, *"Theory of Solid Rocket Motors"*, Science and Technology Publishing House, Hanoi, Vietnam, (2016).

[4]. Trien D. H., Thanh N. T., *"Application of the Inverse Internal Ballistics Problem for the Design of Replacement Propellant Charges in Solid Motors"*, Journal of Military Science and Technology, pp. 137–144, (2007).

[5]. Thanh N. T., Dung H. T., et al., *"Study on the Effect of Pressure on the Thrust Force of a Solid Propellant Engine Operating in a Water Environment"*, Journal of Military Science and Technology, vol. 102, pp. 137–144, (2025).

[6]. Hoang T. Dung, *"Investigation of the Effects of Combustion Chamber Parameters on the Performance*

Characteristics of Solid Motors", Ph.D. Dissertation, Institute of Military Science and Technology, Hanoi, Vietnam, (2018).
[7]. Le S. Tung, Hoang T. Dung, *"Fundamentals of Calculation and Design of Solid Propellant Engines"*, People's Army Publishing House, Hanoi, Vietnam, (2015).
[8]. Орлов Б. В., *"Термодинамические и баллистические основы проектирования РДТТ"*, Издательство Машиностроение, Москва, (1968).
[9]. *"Переносный противотанковый комплекс 9К111 – Техническое описание"*, Военное издательство Министерства обороны СССР, Москва, (1981).
[10]. *"Техническое описание и инструкция по эксплуатации ПТУРС 9М111М"*, Военное издательство Министерства обороны СССР, Москва, (1975).

TÓM TẮT

Nghiên cứu tính toán thuật phóng trong động cơ nhiên liệu rắn hoạt động trong môi trường nước khi kể đến kết cấu nắp bịt kín bảo vệ loa phụt

Bài báo nghiên cứu hoạt động của động cơ nhiên liệu rắn khi hoạt động trong môi trường nước khi xét tới ảnh hưởng của kết cấu nắp bịt kín bảo vệ nước cho động cơ. Hệ phương trình tính toán thuật phóng trong của động cơ nhiên liệu rắn khi kể đến giai đoạn áp lực phá vỡ nắp bảo vệ. Trong giai đoạn hoạt động này thuốc phóng cháy một phần làm tăng áp suất buồng đốt phá vỡ nắp bịt áp suất, một phần khí thuốc tràn vào khoang hình thành bởi nắp bịt kín và loa phụt làm tăng áp suất của khoang này. Khi áp suất khoang thấp áp đủ lớn cắt chốt giữ nắp bịt kín và đẩy nắp chuyển động. Khi nắp bịt kín văng ra ngoài khí thuốc từ buồng đốt phun qua loa ra môi trường hoạt động như động cơ rắn thông thường. Bài báo là cơ sở để tính toán, thiết kế, chế tạo kết cấu thực của động cơ nhiên liệu rắn hoạt động trong môi trường nước.

Từ khóa: Động cơ nhiên liệu rắn; Động cơ hoạt động dưới nước; Buồng cao áp; Buồng thấp áp; Thuật phóng trong.